Available at www.sciencedirect.com

ScienceDirect

journal homepage: www.elsevier.com/locate/he

ELSEVIER

# Formation and hydrogen storage properties of in situ prepared Mg–Cu alloy nanoparticles by arc discharge

J.P. Lei [a], H. Huang [a], X.L. Dong [a],*, J.P. Sun [a], B. Lu [a], M.K. Lei [a], Q. Wang [a], C. Dong [a], G.Z. Cao [b]

[a] School of Materials Science and Engineering, Dalian University of Technology, Dalian, Liaoning 116023, China
[b] Department of Materials Science and Engineering, University of Washington, Seattle, WA 98195, USA

## ARTICLE INFO

## ABSTRACT

Mg–Cu alloy nanoparticles were in situ prepared by a physical vapor condensation method (arc discharge) in a mixture of argon and hydrogen. Four crystalline phases, Mg, $Mg_2Cu$, $MgCu_2$ and MgO, were formed simultaneously during the arc-discharge evaporation. Detailed experiments revealed that nanostructured hydrogen-active phases of $Mg_2Cu$ and Mg exhibit enhanced hydrogen absorption kinetics possibly due to the small grain size and surface defects. The maximal hydrogen storage contents of Mg–Cu alloy nanoparticles can reach $2.05 \pm 0.10$ wt% at 623 K.

## 1. Introduction

The storage of hydrogen gas is presently accomplished with the stainless steel cylinders under high pressure, which is safety hazardous with low gravimetric storage density. In addition, with such gas storage techniques, it is difficult to achieve a storage capacity of 2 wt.% $H_2$. Hydrides are promising hydrogen storage material as gases typically take 1000 times of the space of their solid form. For example, magnesium hydride can store 7 wt.% $H_2$. However, it suffers some drawbacks, such as $MgH_2$ possesses slow hydrogenation and dehydrogenation kinetics, and high release temperature due to its high enthalpy of formation. Alloying magnesium with other elements could lower the stability of the hydride without reducing the capacity to an unacceptable value. The $Mg_2Cu$ alloy, which crystallizes in the orthorhombic structure, is lighter and cheaper than the LaNi5-type alloys. The hydrogen content in $Mg_2Cu$ alloy is also relatively high, being 2.6 wt.% [1], whereas only 1.5 wt.% in LaNi5H6. In the past 30 years, many new developments have occurred in metal hydrides. A breakthrough in hydrogen storage technology was achieved by preparing nanocrystalline hydrides using new non-conventional methods, such as mechanical alloying (MA) [2–5], hydriding combustion synthesis (HCS) [6–8], hydriding chemical vapor deposition (HCVD) [9,10], repetitive-rolling [11,12], etc. As a common characteristic in those methods mentioned above, nano-structured hydride alloys become a flashpoint because of its enhanced kinetics and possibly improvement in thermodynamics, compared to conventional cast alloys [13–15].

Reducing the size of metal hydride particles to form nanoparticles leads to a dramatic change in their physical and chemical properties and became the starting point in most

metal hydride investigations. Shao et al. [16] prepared $Mg_2Cu$ nanoparticles by a two-step method, i.e. nanoparticles of Mg and Cu were separately fabricated by the arc-discharge method and then $Mg_2Cu$ nanoparticles were synthesized by annealing them at a certain temperature under 4.0 MPa hydrogen pressure. In this work, Mg–Cu alloy nanoparticles containing hydrogen-active phases of $Mg_2Cu$ and Mg were prepared *in situ* by a modified arc-discharge method. As a novel one-step and *in situ* synthesis method, this route is significant in many characters, such as short synthesizing time, low impurity, high effectiveness, simply operation, easy to automatize, etc. In this work, the phase, composition, microstructure and morphology of nanoparticles were carefully characterized by various analytical techniques and the formation for multi-phased nanoparticles was also discussed in detail. Hydrogen absorption/desorption properties were investigated by a volumetric method. It is expected to obtain some understandings on the vapor phase synthesized Mg–Cu nanoparticles and its novel hydrogen storage properties.

## 2. Experimental method

The experimental equipment for production of Mg–Cu alloy nanoparticles was similar to our previous work [17]. In the experimental setup a tungsten rod was used as the cathode. Micron-sized Mg and Cu particles (99% purity) were weighed pro rata and compressed into a cylindrical block which served as the anode to be evaporated. Considering the stoichiometric composition of $Mg_2Cu$, the molar ratio of Mg to Cu in raw material (the cylindrical block) was set as 2:1. After evacuating, a mixture of hydrogen and argon was introduced into the work chamber as the source of hydrogen plasma and the condensing atmosphere. Arc current and voltage were maintained at 240 A and 30 V, respectively. Before removing the nanocomposite particles from the chamber, a passivation procedure was carried out on the as-prepared nanoparticles by introduction of a mixture gas of argon and trace air into the chamber for 30 h. The phases in nanoparticles were determined by X-ray diffraction (XRD) using a Shimazu XRD-6000 instrument. The morphology, size and microstructure of the nanoparticles were observed by high-resolution transmission electron microscopy (HRTEM) using a Tecnai220 S-TWIM instrument. The composition in as-prepared Mg–Cu alloy nanoparticles was detected using an energy dispersive spectroscopy (EDS) attachment on TEM. Using a Sieverts' apparatus [18], Mg–Cu alloy nanoparticles were sufficiently activated under a thermal treatment condition, i.e. heating at 673 K for 2 h in 3.0 MPa hydrogen atmosphere and then annealing at the same temperature for 2 h in vacuum. After activation, Pressure–Composition–Isothermal (PCI) curves were measured at different temperatures.

## 3. Results and discussion

### 3.1. Evolvement of Mg–Cu nanoparticles by hydrogen treatment

Fig. 1(A–C) shows X-ray diffraction patterns of Mg–Cu nanoparticles and its varieties through hydrogenation treatments.
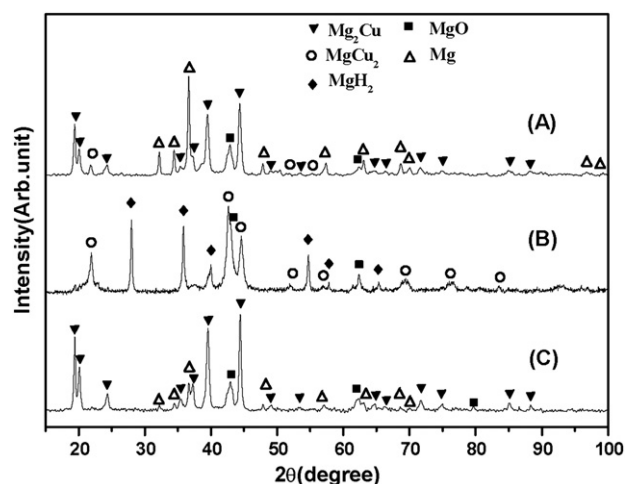


Fig. 1 – XRD patterns of Mg–Cu alloy nanoparticles: (A) as-prepared; (B) after the first hydrogenation process; (C) after 4 cycles of hydrogenation and dehydrogenation.

Four phases, i.e. Mg, $Mg_2Cu$, MgO and $MgCu_2$, coexist in the as-prepared powders (Fig. 1(A)). Discerning the differences in the relative intensities among the diffraction peaks of four phases, it is found that the main phase is metal Mg. EDS analysis indicates that the content of Mg in the as-prepared nano-composite particles (Mg/Cu = 4.2: 1 in molar ratio) becomes excessive with respect to the nominated one in the raw material (Mg/Cu = 2: 1 in molar ratio). From the equilibrium phase diagram [19], there are two kinds of intermetallic compounds ($Mg_2Cu$ and $MgCu_2$) existed in bulk Mg–Cu alloys. In present nanocomposite particles which were synthesized by a non-equilibrium method, the same species of intermetallic compounds are totally detected. Actually, co-existence of $Mg_2Cu$ and $MgCu_2$ is a common phenomenon in nanoparticles of Mg–Cu prepared by other methods, such as the combustion synthesis and annealing of the mixture of pure Mg and Cu nanoparticles [8,16]. The presence of MgO in nanoparticles is ascribed to be originated from the oxidation of Mg during particles' passivation. In the present work, it is difficult to form the single phase of $Mg_2Cu$ in nanoparticles by co-evaporating of magnesium and copper raw materials, although the stoichiometric composition of $Mg_2Cu$ was fixed in the target bulk. In our previous research on Fe–Sn nanoparticles system [17], an excess Sn was also found in such binary alloy system in which there are large differences in the vapor pressures and melting points of two components. It is recognized that the element with relatively high vapor pressure and melting point would be excessive in the resultant nanoparticles of binary alloy, such as Mg–Cu and Sn–Fe alloy systems in which two constituting elements have great diversities in their characters.

Hydrogenation treatments include the activation process (three hydriding/dehydriding cycles) and P–C–I measurement. XRD patterns of the treated Mg–Cu nanoparticles after the first hydrogenation and 4 cycles of hydrogenation and dehydrogenation are also presented as Fig. 1(B) and (C), respectively. After the first hydrogenation reaction, three phases $MgCu_2$, $MgH_2$ and MgO coexist. However, the amounts of $Mg_2Cu$ and

Mg decreased noticeably and disappeared as shown in Fig. 1(B). Pure Mg phase was completely hydrogenated to form $MgH_2$ and the phase of $Mg_2Cu$ reacted with hydrogen to form $MgCu_2$ and $MgH_2$. Pure Mg and $Mg_2Cu$ were recovered after several hydrogenation and dehydrogenation cycles as shown in Fig. 1(C). These results suppose the reaction mechanism and phase transformations occurred in the process of hydrogen absorption/desorption, and can be formulized as follows [1]:

$$Mg + H_2 \leftrightarrow MgH_2 \tag{1}$$

$$2Mg_2Cu + 3H_2 \leftrightarrow MgCu_2 + 3MgH_2 \tag{2}$$

It can be recognized that the hydrogenation was carried out on both of active phases of Mg and $Mg_2Cu$ in the Mg–Cu nanoparticles. Calculation from XRD peaks by using of Scherer equation revealed that the average grain sizes are approximately 38, 27, 24, and 27 nm for Mg, $Mg_2Cu$, $MgCu_2$ and MgO phases in the as-prepared nanocomposite particles, respectively; and changed to approximately 10, 16 and 15 nm for $MgCu_2$, $MgH_2$ and MgO phases after first hydrogenation process. After 4th cycle of hydrogenation and dehydrogenation, they are approximately 30, 36 and 26 nm for Mg, $Mg_2Cu$ and MgO phases, respectively. These results imply that the phase transition or hydrogenation and dehydrogenation resulted in an increased grain size of $Mg_2Cu$. Although the mechanism of such a change of grain size is not known, it is possible that an aggregation and grain boundary diffusion may occur during the hydrogenation and dehydrogenation reactions, leading to an increased grain size.

Fig. 2 (A) and (B) presents morphologies and core/shell interface in the as-prepared Mg–Cu nanoparticles in different magnifications. Nanoparticles are spherical in shape with its sizes ranging from 50 nm to 350 nm. The rectangle region labeled in Fig. 2(A) is magnified for detailed analysis on the shell/core structure of nanoparticles (Fig. 2(B)). The shell of nanoparticles is identified as a crystal MgO with the interplanar spacing of 0.21 nm for (200) plane. Similarly, $Mg_2Cu$ and $MgCu_2$ are also detected as part of the core of nanoparticles by their interplanar spacings, i.e. 0.23 nm for $Mg_2Cu$ (080) plane and 0.21 nm for $MgCu_2$ (311) plane. The detailed mechanism for such core/shell structure in Mg–Cu nanoparticles will be discussed in the next Section 3.2. Evaluating from TEM micrographs, the mean size is approximately 144 nm for the as-prepared Mg–Cu nanoparticles. In brief, three prominent characteristics of the as-prepared nanoparticles can be obtained from Fig. 2, i.e. smooth particle's surface, larger average particles' size and polycrystalline structure in a single nanoparticle.

In order to investigate the effect of hydrogenation treatment on the morphologies and microstructures, the treated Mg–Cu nanoparticles after several hydriding/dehydriding cycles were analyzed by HRTEM observations as shown in Fig. 3(A–C). By the lattice fringe analysis, $Mg_2Cu$ compound and MgO are identified as core and shell of a nanoparticle, respectively. In comparison with as-prepared nanoparticles, three obvious changes associated with morphologies and microstructures are observed after hydrogenation treatment. First, some partially hollow nanoparticles appear as labeled with arrows (Fig. 3(A)). Second, interspaces between core and shell are observed in one nanoparticle, which is the bright image area (Fig. 3(B)). Third, serious pulverization of nanoparticles occurred during hydrogenation/dehydrogenation cycle. As a result of pulverization, one nanoparticle was crushed into several smaller sized particles. The initial size of Mg–Cu nanoparticles was in the range of 50–350 nm which was then changed as about 5–270 nm after several hydrogenation/dehydrogenation processes. Meanwhile, other phenomena were emerged, such as irregular shape, partially hollow nanoparticles, the presence of some particles with smaller size, the separation between shell and core, etc.

## 3.2. Formation and derivation of Mg–Cu alloy nanoparticles

As discussed in Section 3.1, intermetallic compounds ($Mg_2Cu$ and $MgCu_2$) in as-prepared Mg–Cu nanoparticles were confirmed by XRD diffraction (Fig. 1(A)). In arc-discharge,
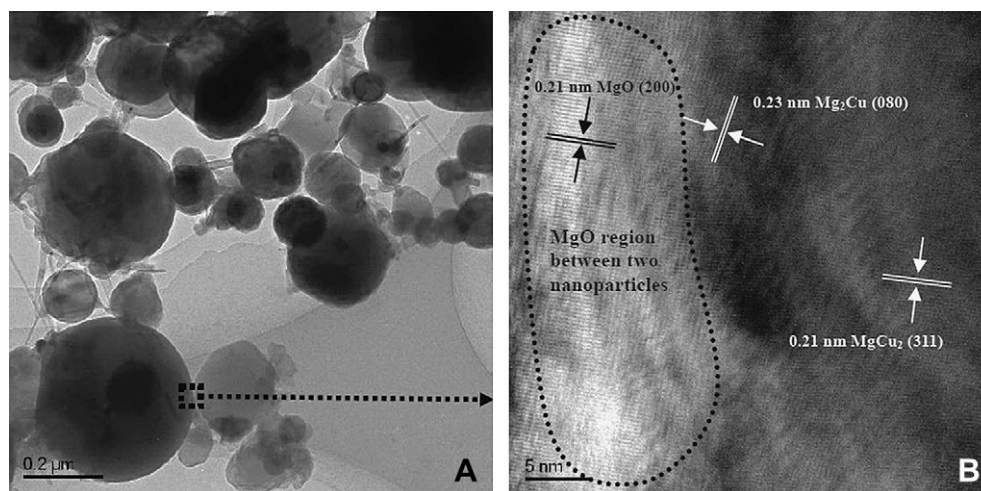


Fig. 2 – (A) TEM image of the as-prepared Mg–Cu nanoparticles; (B) HRTEM image of the region labeled by a rectangle in image (A).
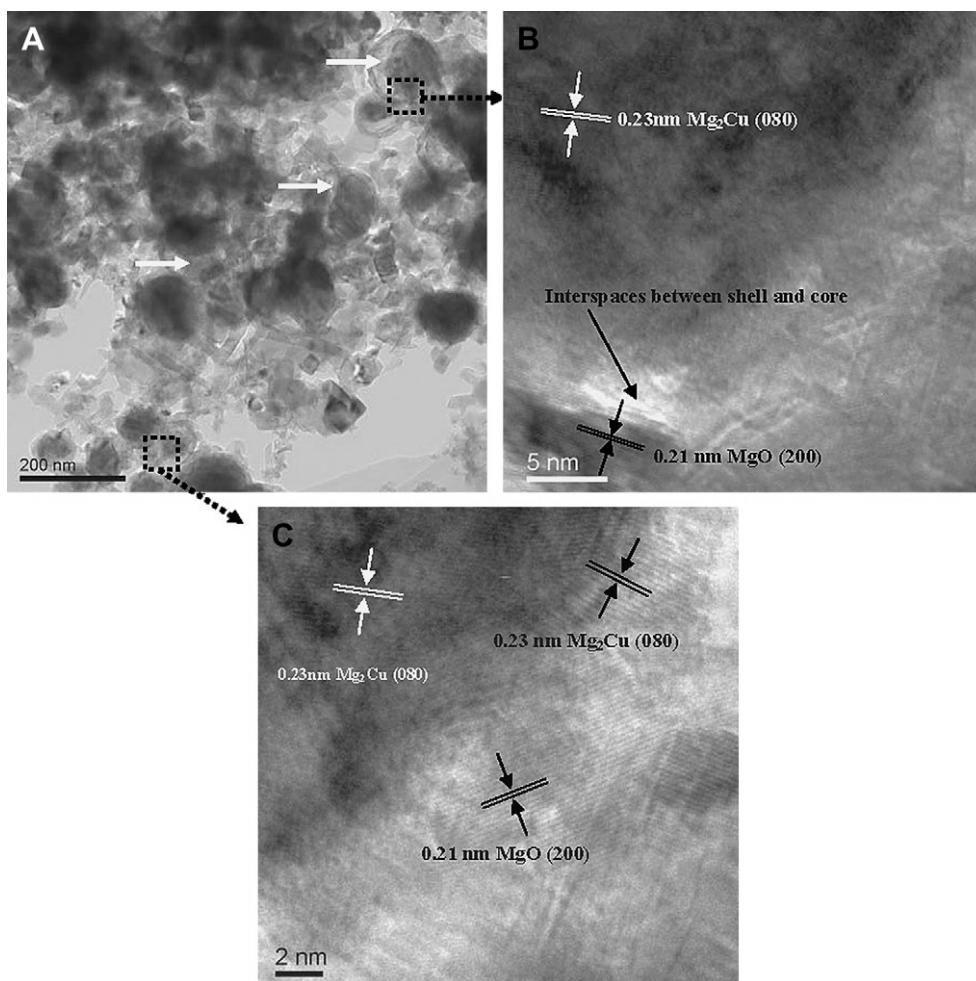
**Fig. 3 – Pulverization and microstructure's change in Mg–Cu alloy nanoparticles by the hydrogenation/dehydrogenation processes.**

a typical physical gas-phase method, the nanoparticles arised from a vapor condensation process involving evaporation, nucleation and growth. According to the conventional theory on nucleation and growth, it can be speculated that there are six stages through all the formation of Mg–Cu nanoparticles. A schematic diagram concerning the formation of Mg–Cu nanoparticles is illustrated in Fig. 4. First, individual atoms of Mg and Cu will co-exist in gas state above the boiling point of Cu ($T_{b, Cu}$) because Mg has a lower boiling temperature than Cu, as shown in Fig. 4(A). Second, homogeneous nucleation is expected in an arc-discharge condition in which there are no preferential sites for nucleation. Prior to Mg elements, Cu atoms favor to form bigger clusters surrounding by gaseous Mg atoms in the temperature range from $T_{m, Cu}$ to $T_{b, Cu}$ (Fig. 4(B)). Third, Cu clusters are collided to be nuclei in a temperature between $T_{b, Mg}$ and $T_{m, Cu}$ (Fig. 4(C)). Fourth, above melting point of Mg ($T_{m, Mg}$), the grown Cu particles provide favorable sites for a heterogeneous nucleation of Mg and grow to larger composite particles in nanometer scale. Simultaneously, intermetallic $Mg_2Cu$ compound is created through the interface reaction and diffusion (Fig. 4(D)). At the temperature below than melting point of Mg, all phases in

particles, i.e. Mg, $Mg_2Cu$ and $MgCu_2$, are formed by solid diffusion (Fig. 4(E)). After passivation process, MgO layer forms on the surface of nanoparticles (Fig. 4(F)). It should be mentioned on the sequence of formation for $Mg_2Cu$ and $MgCu_2$ phases. From Mg–Cu alloy phase diagram [18], it is known that $Mg_2Cu$ emerges firstly as Mg become excessive. Frederick et al. [20] experimentally found that $Mg_2Cu$ is the primary phase in the as-prepared Cu–Mg film with excessive Mg content than the stoichiometric composition of $Mg_2Cu$. Therefore, it is also reasonably speculated that $Mg_2Cu$ is the primary phase in the present work.

Evolvement of Mg–Cu nanoparticles by the hydrogenation treatment can be schematically illustrated as shown in Fig. 5. As proved by XRD diffraction patterns (Fig. 1), the hydriding/dehydriding process can cause phase transitions which is usually characterized by a crystalline structure change, a volume expansion/shrinkage, and a nucleation energy barrier [14]. In the hydrogenation process, it is believed that the volume expansion takes place as long as existence of active phases and volume shrinkage also occurs in the dehydriding process (Fig. 5(A) and (B)). Calculating from the theory density of active phases indicates that volume changes during
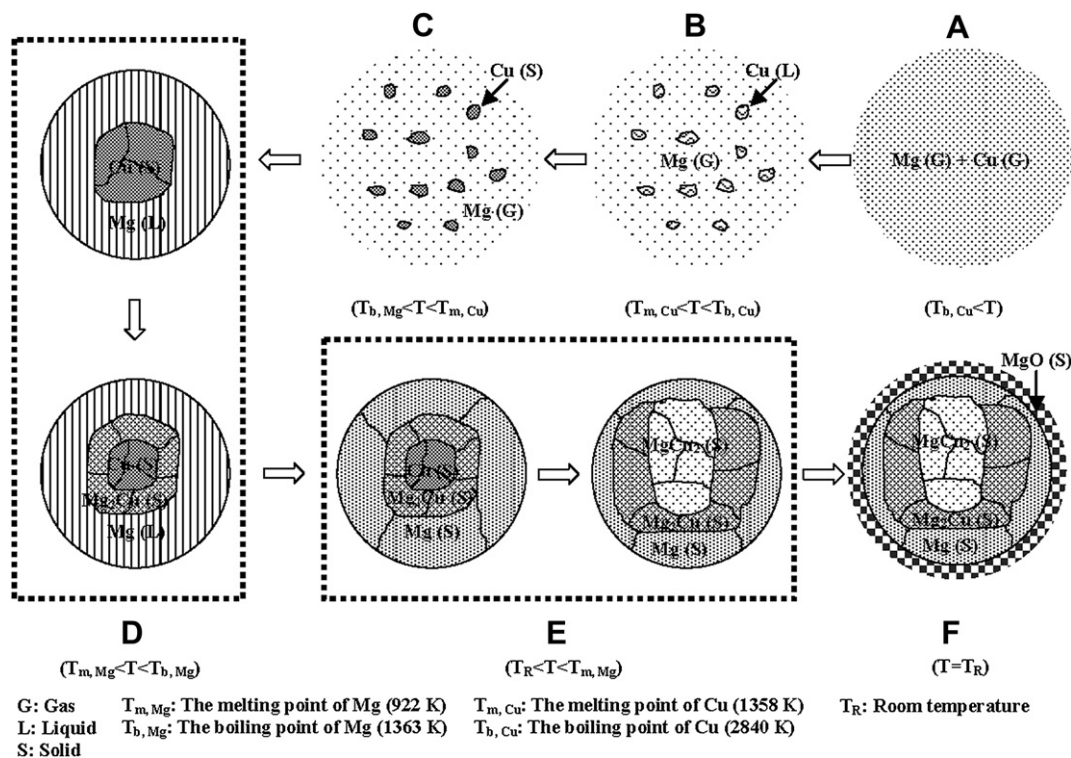
**Fig. 4 – A schematic diagram for the possible formation mechanism of Mg–Cu alloy nanoparticles.**

hydrogenation process are 33% for reaction Eq. (1) and 24% for Eq. (2). The hydrogenation process is complex and involves multi-sequential and yet parallel steps. The applied activation procedure includes penetration of the surface MgO oxide layer, hydrogenation, and propagation from surface to inner core, leading to cracking of particles, due to the expansion of crystal lattice associated with the hydride formation and the brittle nature of the hydride [21]. It is known that hydrogen diffusion in the close packed MgO is extremely slow [22] and strongly thermally activated compared to diffusion of hydrogen in Mg [23] and MgH$_2$ [24]. As inactive phase and shell of Mg–Cu nanoparticles, MgO has tendency to keep original morphologies and cause the separation between shell (MgO) and core (active phases) or partly hollow particles.

Other factor to be considered is the diffusion of hydrogen atoms, whose movement along grain boundaries is usually faster than that inside the lattice due to the lower packing density and defects in interfaces. Thus, grain boundaries would be the favorable nucleation sites for the hydride phase. In such case, it is reasonable to suppose that pulverization of nanoparticle is initiated at grain boundaries by the volume changes (Fig. 5(C)) and the separation among polycrystalline grains occurs. Here, it should be noted that the presence of MgO is not always unfavorable which appears to exert a stabilizing effect on stability as hydrogen storage [25]. It is expected that MgO can constrain growth of the cracked particles in subsequent cycles of hydrogenation treatment. Aguey-Zinsou et al. [26] found that the hydrogen storage properties of Mg can be significantly improved by mechanical milling MgH$_2$ with doping MgO, in which MgO exhibits good lubricant and dispersing properties as well as the stimulative

effect on further decrease of MgH$_2$ particles size. It had been indicated that the pulverization of nanoparticles, phase transition and presence of MgO may play positive effects on improvement of hydrogen absorption kinetics and prohibition of recrystallization in cracked nanoparticles [26]. Furthermore, the smaller sizes of grains or particles created by pulverization will bring out lots of defects, i.e. new fresh surfaces, boundaries, etc. and can reduce the diffusion distances and increase the surface areas, which all facilitate the hydriding/dehydriding process and improve the hydrogen storage properties.

### 3.3. Hydrogen absorption properties of Mg–Cu alloy nanoparticles

#### 3.3.1. Hydrogen absorption kinetics

From a thermodynamic view, Mg-based hydrides should form readily at room temperature. However, this case never occur in practice because of kinetic limitations [27]. Generally, a typical hydrogen absorption process for the overall reaction is composed of five intermediate partial processes, i.e. physisorption, chemisorption, surface penetration, diffusion, and hydrides formation [28]. Any delay of those processes will reduce the kinetic properties. The presence of MgO surface layer for Mg-based alloy is usually unavoidable due to air exposure or oxygen impurity in H$_2$ gas. MgO layer on the surface of nanoparticles are not transparent to hydrogen molecules and consequently prevents hydrogen molecules from penetrating into the material. To initiate hydrogen absorption the MgO layer must be perforated or cracked, which is the essence of activation. Here, the activation was
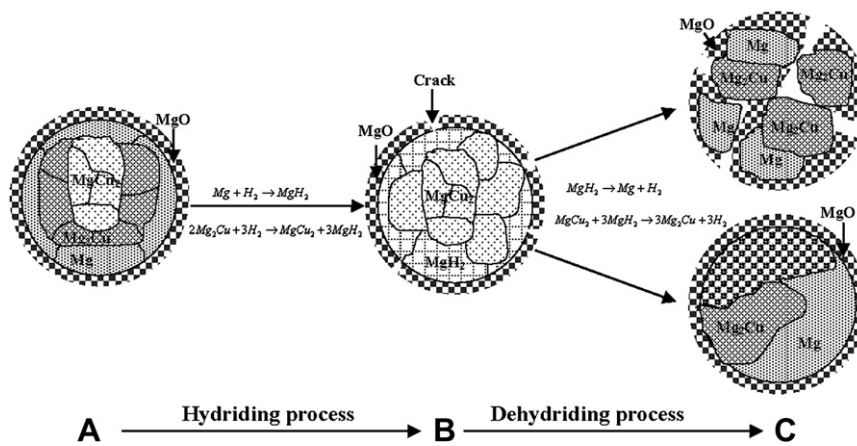
Fig. 5 – A schematic diagram for the hydrogenation/dehydrogenation process.

carried out at 673 K under 3.0 MPa of hydrogen pressure. For dehydrogenation process, samples were annealed at the same temperature in vacuum and the finish of hydrogen desorption was reached when the change of hydrogen pressure was less than about 1 Pa per minute. Fig. 6 is the hydrogenation kinetic curves for Mg–Cu nanoparticles. Especially, the curve for cycle 1 presents the effect of activation on hydrogen absorption kinetics for the as-prepared Mg–Cu nanoparticles, which is a typical sigmoidal shape and can be well explained by the conventional theory of Johnson–Mehl–Avrami for nucleation and growth [29]. The reason for this behavior, however, is not internal kinetics but successive activation of the sample's surface [30].

Prior to be measured, the hydrogenated sample was annealed for 2 h in vacuum at 673 K for the purpose of completely dehydrogenation. There are two significant changes observed in Fig. 6. On one hand, the maximum hydrogen absorption content is reached in cycle 1, i.e.
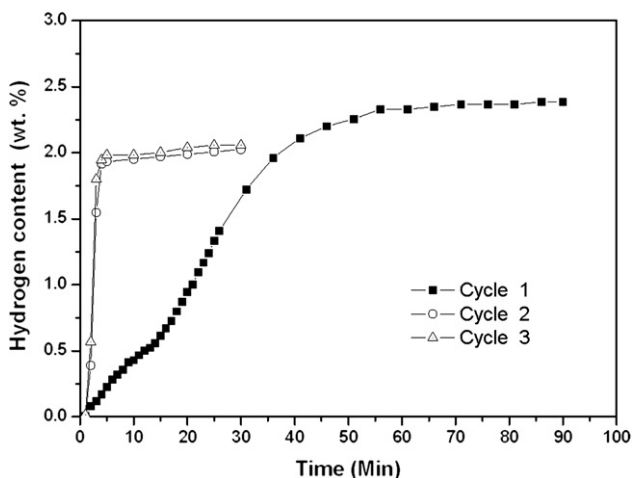
2.38 ± 0.19 wt.% of hydrogen in 90 min. Meanwhile, the saturated hydrogen absorptions are 2.02 ± 0.16 wt.% and 2.06 ± 0.16 wt.% for cycle 2 and cycle 3, respectively. In normal case for a hydrogen storage material, the maximum hydrogen absorption contents are almost the same among the cycles, or it is lower for the first cycle due to an incompletely hydrogen activating. In present Mg–Cu nanoparticles, the situation is quite contrary implying that there are multi phases coexisted. Actually, the first cycle is an activation process and the higher hydrogen absorption content is attributed to the existence of excessive Mg as indicated by XRD (Fig. 1A). It is well known that pure Mg can absorb 7.6 wt.% of hydrogen at maximum. In cycles 2 and 3, the quantities of Mg became relatively lower owing to the phase transformation by hydrogen treatment, i.e. decrease of Mg content accompanying with an increase of $Mg_2Cu$ after hydrogen treatment (Fig. 1C). On the other hand, the hydrogen absorption rates for both of the cycles 2 and 3 are obviously higher than that in cycle 1. It is also found that all hydrogen absorption rates of cycles for Mg–Cu nanoparticles are higher than that for melting–casting alloys [12], exhibiting a better reaction kinetics. The hydrogen absorption contents reach 0.23 ± 0.02 wt.% in 5 min during the first cycle, while it is 1.93 ± 0.15 wt.% and 1.98 ± 0.16 wt.% for the cycles 2 and 3, respectively.

As known from the above results, the hydrogenation kinetics for nanoparticles is improved by a simple activation with only one thermal cycling, which is a consequence of several combined effects. Firstly, an abundance of defects and boundaries exist in the nanostructured particles, such as phase boundaries, interfaces of core/shell structure, dislocations, etc., and all of them favor to store an excess energy and further facilitate hydrogen absorption. In other words, the presence of grain boundaries and defects allow hydrogen atoms to easily penetrate into nanoparticles. Secondly, the broken MgO shells may bring a positive effect on improvement of hydrogen absorption kinetics by promoting the nucleation of hydrides at interfaces between MgO and Mg phases. It was also proved that a thin and defective MgO layer can improve hydrogen absorption rate for Mg-based alloys [31]. Andreasen et al. reported that improved oxidation resistance was obtained in Mg–Cu complex compared to pure Mg



Fig. 6 – Hydrogen absorption kinetic curves of Mg–Cu alloy nanoparticles. Cycle 1 is the hydrogen activation on the as-prepared nanoparticles, cycles 2 and 3 are the successive hydrogenation processes.

sample due to the presence of $Mg_2Cu/MgCu_2$ [21]. The effect of MgO layer was rationalized within the concept of ''Process Control Agent'' and its efficiency of MgO for decreasing the growth rate of Mg crystallites during cycling (periodic hydriding–dehydriding) was tested [32]. In this study, the positive effect of MgO shell in Mg–Cu nanoparticles on the hydrogenation kinetics is also expected.

### 3.3.2. P–C–I curves of Mg–Cu alloy nanoparticles

P–C–I curves were measured at different temperature to reveal hydrogenation/dehydrogenation properties of Mg–Cu nanoparticles, as shown in Fig. 7. After activation processes, the as-prepared Mg–Cu nanoparticles become a new composite containing two main active phases of $Mg_2Cu$ and Mg (Fig. 1C). Accordingly, P–C–I curves exhibit two plateaus corresponding to the hydrogen absorption reactions of Mg (at lower pressure) and $Mg_2Cu$ (at higher pressure), respectively [1]. The hydrogen absorption contents at higher pressure are $1.92 \pm 0.10$, $1.98 \pm 0.10$ and $2.05 \pm 0.10$ wt.% at 573, 598 and 623 K, and at lower pressure are $0.64 \pm 0.03$, $0.56 \pm 0.03$ and $0.53 \pm 0.03$ wt.% at 623, 598 and 573 K, respectively. The maximum hydrogen uptake of $Mg_2Cu$ phase at 623 K is 2.05 wt.%, which is a little lower than 2.25 wt.% of nanocrystalline $Mg_2Cu$-type alloys synthesized by mechanical alloying and annealing [5]. These results show a tendency that the hydrogen absorption content is improved by a gradually increased temperature. On basis of a classical analysis, the hydrogen solubility in $Mg_2Cu$ nanoparticles is expected to be decreased at a higher temperature and reflected in the length of corresponding plateau in P–C–I curve [19]. On the contrary, the present results on Mg–Cu nanoparticles display an inverse behavior with the classical analysis. This phenomenon may be attributed to the presence of Mg component which has poor hydrogen absorption kinetic at lower temperature [33]. It is reasonable to recognize that some kinetics factors may restrict the hydrogenation reaction of Mg at low temperature and result in the present phenomenon.
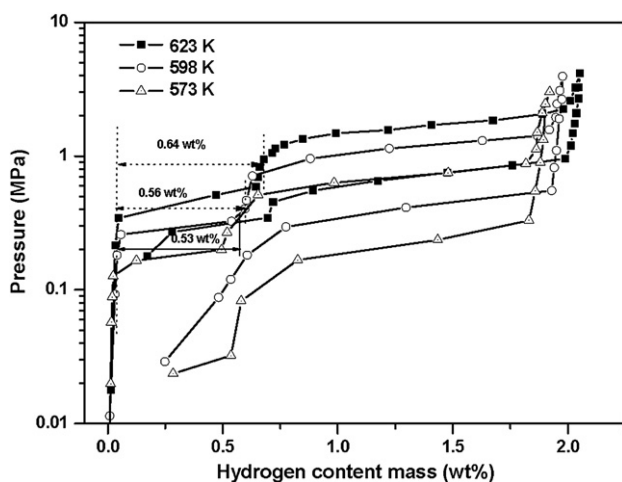


**Fig. 7 – P–C–I curves of Mg–Cu alloy nanoparticles at different temperatures. The plateaus represent the hydrogen absorption reactions of Mg (at lower pressure) and $Mg_2Cu$ (at higher pressure).**

## 4. Conclusions

Mg–Cu alloy nanoparticles were *in situ* prepared by an arc-discharge method using micro-sized metallic powders of Mg and Cu as the raw materials. Four phases, i.e. intermetallic compounds of $Mg_2Cu$ and $MgCu_2$, Mg and MgO, coexist in an Mg–Cu nanoparticle. As-prepared Mg–Cu nanoparticles have spheral shapes, readily to disintegrate into smaller nano-particles when subjected to hydrogenation. The $Mg_2Cu$ compound, desirable phase for efficient hydrogen storage, increases in content and becomes a main phase through the phase transformation after several cycles of hydrogenation and dehydrogenation. Mg–Cu alloy nanoparticles exhibit an excellent kinetic property with higher hydrogen absorption rate due to its high specific surface area and the defects. The co-existence of other metal or metal compound phases may serve as an easy path for quick heat transfer during the hydrogenation and dehydrogenation reactions. The maximal hydrogen storage contents of Mg–Cu alloy nanoparticles are $1.92 \pm 0.10$, $1.98 \pm 0.10$ and $2.05 \pm 0.10$ wt.% at 573, 598 and 623 K, respectively.

### REFERENCES

[1] Reilly JJ, Wiswall RH. The reaction of hydrogen with alloys of magnesium and copper. Inorg Chem 1967;6:2220–3.

[2] Gennari FC, Castro FJ, Urretavizcaya G. Hydrogen desorption behavior from magnesium hydrides synthesized by reactive mechanical alloying. J Alloys Compd 2001;321:46–53.

[3] Liang G. Synthesis and hydrogen storage properties of Mg-based alloys. J Alloys Compd 2004;370:123–8.

[4] Ivanov E, Konstanchuk I, Stepanov A, Boldyrev V. Magnesium mechanical alloys for hydrogen storage. J Less Common Met 1987;131:25–9.

[5] Jurczyk M, Okonska I, Iwasieczko W, Jankowska E, Drulis H. Thermodynamic and electrochemical properties of nanocrystalline $Mg_2Cu$-type hydrogen storage materials. J Alloys Compd 2007;429:316–20.

[6] Akiyama T, Isogai H, Yagi J. Hydriding combustion synthesis for the production of hydrogen storage alloy. J Alloys Compd 1997;252:L1–4.

[7] Li LQ, Akiyama T, Yagi JI. Reaction mechanism of hydriding combustion synthesis of $Mg_2NiH_4$. Intermetallics 1999;7: 671–7.

[8] Li LQ, Saita I, Saito K, Akiyama T. Hydriding combustion synthesis of hydrogen storage alloys of Mg–Ni–Cu system. Intermetallics 2002;10:927–32.

[9] Saita I, Toshima T, Tanda S, Akiyama T. Hydriding chemical vapor deposition of metal hydride nano-fibers. Mater Trans 2006;47:931–4.

[10] Saita I, Toshima T, Tanda S, Akiyama T. Hydrogen storage property of $MgH_2$ synthesized by hydriding chemical vapor deposition. J Alloys Compd 2007;446:80–3.

[11] Ueda TT, Tsukahara M, Kamiya Y, Kikuchi S. Preparation and hydrogen storage properties of Mg–Ni–Mg$_2$Ni laminate composites. J Alloys Compd 2005;386:253–7.

[12] Takeichi N, Tanaka K, Tanaka H, Ueda TT, Kamiya Y, Tsukahara M, et al. Hydrogen storage properties of Mg/Cu and Mg/Pd laminate composites and metallographic structure. J Alloys Compd 2007;446:543–8.

[13] Orimo S, Fujii H. Effects of nanometer-scale structure on hydriding properties of Mg–Ni alloys: a review. Intermetallics 1998;6:185–92.

[14] Bérubé V, Radtke G, Dresselhaus M, Chen G. Size effects on the hydrogen storage properties of nanostructured metal hydrides: a review. Int J Energy Res 2007;31:637–63.

[15] Jurczyk M, Smardz L, Okonska I, Jankowska E, Nowak M, Smardz K. Nanoscale Mg-based materials for hydrogen storage. Int J Hydrogen Energy 2008;33:374–80.

[16] Shao HY, Wang YT, Xu HR, Li XG. Preparation and hydrogen storage properties of nanostructured Mg$_2$Cu alloy. J Solid State Chem 2005;178:2211–7.

[17] Lei JP, Dong XL, Zhu XG, Lei MK, Huang H, Zhang XF, et al. Formation and characterization of intermetallic Fe–Sn nanoparticles synthesized by an arc discharge method. Intermetallics 2007;15:1589–94.

[18] David L, Sandrine BF, José GA, Laurent F, Patrick A. Development of a volumetric method-experimental test bench for hydrogen storage characterization. Int J Hydrogen Energy 2007;32:1846–54.

[19] Zhou SH, Wang Y, Shi FG, Sommer F, Chen LQ, Liu ZK, et al. Modeling of thermodynamic properties and phase equilibria for the Cu–Mg binary system. JPEDAV 2007;28:158–66.

[20] Frederick MJ, Goswami R, Ramanath G. Sequence of Mg segregation, grain growth, and interfacial MgO formation in Cu–Mg alloy films on SiO$_2$ during vacuum annealing. J Appl Phys 2003;93:5966–72.

[21] Andreasen A, Sørensen MB, Burkarl R, Møller B, Molenbroek AM, Pedersen AS, et al. Dehydrogenation kinetics of air-exposed MgH2/Mg2Cu and MgH2/MgCu2 studied with in situ X-ray powder diffraction. Appl Phys A 2006;82:515–21.

[22] Gonzalez R, Chen Y, Tsang KL. Diffusion of deuterium and hydrogen in doped and undoped MgO crystals. Phys Rev B 1982;26(8):4637–45.

[23] Vegge T. Locating the rate-limiting step for the interaction of hydrogen with Mg (001) using density-functional theory calculations and rate theory. Phys Rev B 2004;70. 035412.

[24] Töpler J, Buchner H, Säufferer H, Knorr K, Prandl W. Measurements of the diffusion of hydrogen atoms in magnesium and Mg$_2$Ni by neutron scattering. J Less Common Met 1982;88:397–404.

[25] Ostenfeld CW, Chorkendorff IB. Effect of oxygen on the hydrogenation properties of magnesium films. Surf Sci 2006; 600:1363–8.

[26] Aguey-Zinsou KF, Ares Fernandez JR, Klassen T, Bormann R. Using MgO to improve the (de)hydriding properties of magnesium. Mater Res Bull 2006;41:1118–26.

[27] Zaluska A, Zaluski L, Strom-Olsen JO. Nanocrystalline magnesium for hydrogen storage. J Alloys Compd 1999;288:217–55.

[28] Martin M, Gommel C, Borkhart C, Fromm E. Absorption and desorption kinetics of hydrogen storage alloys. J Alloys Compd 1996;238:193–201.

[29] Avrami M. Kinetics of phase change. I general theory. J Chem Phys 1939;7:1103–12.

[30] Johnson WA, Mehl RF. Reaction kinetics in processes of nucleation and growth. Trans AIME 1939;135:416–68.

[31] Hjort P, Krozer A, Kasemo B. Hydrogen sorption kinetics in partly oxidized Mg films. J Alloys Compd 1996;237:74–80.

[32] Gerasimov KB, Konstanchuck IG, Chizhik SA, Bobet JL. ''Hysteresis'' in interaction of nanocrystalline magnesium with hydrogen. Int J Hydrogen Energy 2009;34:1916–21.

[33] Shao HY, Wang YT, Xu HR, Li XG. Hydrogen storage properties of magnesium ultrafine particles prepared by hydrogen plasma-metal reaction. Mater Sci Eng B 2004;110:221–6.